SCISPACE
formerly Typeset

Open access • Journal Article • DOI:10.1103/PHYSREVB.75.184421

Nonstoichiometry as a source of magnetism in otherwise nonmagnetic oxides : magnetically interacting cation vacancies and their percolation — Source link

Jorge M. Osorio-Guillén, Stephan Lany, Sergey V. Barabash, Alex Zunger

Institutions: National Renewable Energy Laboratory

Published on: 18 May 2007 - Physical Review B (American Physical Society)

Related papers:

- Ferromagnetism driven by intrinsic point defects in HfO(2).
- Ferromagnetism as a universal feature of nanoparticles of the otherwise nonmagnetic oxides
- Thin films: unexpected magnetism in a dielectric oxide.
- Room-temperature ferromagnetism observed in undoped semiconducting and insulating oxide thin films
- Magnetism without Magnetic Ions: Percolation, Exchange, and Formation Energies of Magnetism-Promoting Intrinsic Defects in CaO

Share this paper:

View more about this paper here: https://typeset.io/papers/nonstoichiometry-as-a-source-of-magnetism-in-otherwise-1o2pzxt431

Nonstoichiometry as a source of magnetism in otherwise nonmagnetic oxides: Magnetically interacting cation vacancies and their percolation

J. Osorio-Guillén, S. Lany, S. V. Barabash, and A. Zunger
National Renewable Energy Laboratory, Golden, Colorado 80401, USA
(Received 20 January 2007; published 18 May 2007)

We discuss the physical conditions required for the creation of collective ferromagnetism in nonmagnetic oxides by intrinsic point defects such as vacancies. We use HfO_2 as a case study because of recent pertinent calculations and observations. It was previously noted theoretically that charge-neutral Hf vacancies in HfO_2 have partially occupied electronic levels within the band gap, and thus the vacancies carry a nonvanishing local magnetic moment. Such density functional supercell calculations have further shown that two such vacancies interact ferromagnetically if they are separated by up to third-neighbor distance. This suggested to the authors that Hf vacancies could explain the observed collective ferromagnetism in thin HfO_2 films. Here we use our previously developed more complete methodology [Phys. Rev. Lett. **96**, 107203 (2006)] to inquire if such vacancies can lead to collective ferromagnetism. Applying this methodology to HfO_2, we find the following: (i) Hf vacancies appear in a few possible charge states but not all of these have a local magnetic moment. (ii) We calculate the energy required to form such vacancies in HfO_2 as a function of the chemical potential and Fermi energy, and from this we compute, as a function of growth temperature and oxygen pressure, the equilibrium concentration of those vacancies that have a nonvanishing local magnetic moment. We find that under the most favorable equilibrium growth conditions the concentration of Hf vacancies with magnetic moment at room temperature does not exceed 6.4×10^{15} cm^{-3} (fractional composition of $x_{eq}=2.2\times10^{-7}%$). (iii) Independently, we calculate the minimum Hf vacancy concentration needed to achieve wall-to-wall percolation in the HfO_2 lattice, given the range of the magnetic V_{Hf}-V_{Hf} interaction (five neighbors) obtained from our supercell calculations. It turns out that the minimum percolation concentration $x_{perc}=13.5%$ needed for collective ferromagnetism is eight orders of magnitude higher than the equilibrium vacancy concentration x_{eq} in HfO_2 under the most favorable growth conditions. We conclude that equilibrium growth cannot lead to ferromagnetism and that ferromagnetism can be established only if one beats the equilibrium Hf vacancy concentration during growth by as much as eight orders of magnitude. This paper presents also an Appendix that gives the Monte Carlo–calculated percolation thresholds of various lattices as a function of the percolation radius of the interaction.

DOI: 10.1103/PhysRevB.75.184421 PACS number(s): 71.15.Mb, 71.55.−i, 75.50.Pp, 64.60.Ak

I. INTRODUCTION

Recently, the possibility of inducing ferromagnetism in nonmagnetic insulators[1–8] and in C_{60}-based systems[9–11] by creating intrinsic point defects, rather than by the more traditional approach of substitution by magnetic ions, has been discussed. Indeed, it appears that such observations of magnetism are invariably occurring in oxide samples having strong structural deviations from crystalline perfection, including heavily epitaxially textured samples and large-surface-area nanostructure grain boundaries, all associated with significant deviation from stoichiometry[12,13]. Here, we critically examine the conditions that may lead to such defect-induced ferromagnetism, following the general procedure we developed[6] for CaO. Our approach is to first find the conditions leading to defect-induced magnetism under equilibrium. This will quantitatively establish the disparity between the defect concentration needed to establish equilibrium magnetism and what one would need to achieve experimentally with deliberate deviations from equilibrium. We outline four steps needed to determine if defect-induced magnetism is possible.

First, one must identify a defect that has, in isolation, a nonvanishing magnetic moment. The simplest case is where a structural defect is stable with partially occupied electron levels. Indeed, in general,[14,15] point defects in insulators can create localized levels in the band gap capable of having different electron occupancies and thus different charge states and magnetic moments. For example, a charge-neutral cation vacancy in divalent monoxides (e.g., MgO, CaO), $V^0_{\text{cation-II}}$, creates a two-hole center, whereas the singly negative vacancy $V^-_{\text{cation-II}}$ has one hole in the e_1 gap level and a doubly negative vacancy $V^{2-}_{\text{cation-II}}$ has a fully occupied e_1 level (no holes).[6] Likewise, the cation vacancy in four-valent oxides (e.g., HfO_2) creates a four-hole center for the charge-neutral center $V^0_{\text{cation-IV}}$ and a fully occupied level for the quadruply negative $V^{4-}_{\text{cation-IV}}$ center. Such partially occupied orbitals ("open shell") may give rise to local magnetic moments. For example, $\mu=2\mu_B$ for $V^0_{\text{cation-II}}$, $\mu=1\mu_B$ for $V^-_{\text{cation-II}}$, and $\mu=4\mu_B$ for $V^0_{\text{cation-IV}}$. However, other charge states may have zero moment—e.g., the maximally occupied $V^{2-}_{\text{cation-II}}$ or $V^{4-}_{\text{cation-IV}}$. For the two-hole $V^0_{\text{cation-II}}$, if the ground state is a singlet (spin $S=0$), the total moment will vanish. Experimentally the $S=1$ triplet configuration has been observed for isolated cation vacancies in CaO and MgO, but the energy ordering between the spin-singlet ($S=0$) and spin-triplet ($S=1$) states has been debated.[16,17]

Many authors have demonstrated via calculations the existence of such nonzero local magnetic moments for isolated open-shell defects. For example, calculations by Elfimov

 ©2007 The American Physical Society

et al.[1] for $V^0_{\text{cation-II}}$ in CaO and by Das Permmaraju and Sanvito[3] for $V^0_{\text{cation-IV}}$ in HfO_2 considered only neutral defects and predicted a nonzero magnetic moment. Another mechanism for creating defects with nonzero moment was proposed by Coey *et al.*[4] who suggested a scenario where, e.g., anion vacancies are polarized by interactions with the magnetic moments of transitions metals and form a spin-polarized impurity-band-mediated ferromagnetic interaction. This scenario requires that the oxygen vacancy levels be sufficiently close to the host-conduction band in order to hybridize with the otherwise nonmagnetic conduction band (made of empty Hf $5d$ states in HfO_2), rendering the latter magnetic.[5] Recent theoretical studies have shown that this is clearly not the case in[18,19] TiO_2 or[6] CaO where the oxygen vacancy level is far below the host conduction band; we will see here that it is not the case in HfO_2 either.

The observation that annealing in O_2 atmosphere reduces or even eliminates the ferromagnetism[5,12] leads to speculations that direct ferromagnetic coupling between oxygen vacancies could be responsible for ferromagnetism. The charge states of V_O that has magnetic moment are 1+ and 1−. Due to the deep and localized nature of the V_O^+ level, such vacancies are not magnetically coupled.[3] We find that the interaction of two V_O^- vacancies is antiferromagnetic and conclude that oxygen vacancies in bulk HfO_2 are not responsible for ferromagnetism.

Second, once an isolated defect leading to a magnetic moment is identified, one must establish that the defect charge state that has such a nonzero magnetic moment is the stable center given the actual Fermi energy $E_F(T)$. Indeed, the formation of charged defects would violate the charge-neutrality condition, so other charge-compensating defects or (charge-carrying) carriers are needed to conserve charge neutrality. For example, anion vacancies (donors) can compensate cation vacancies (acceptors). Various such charged defects as well as thermal excitations of electrons and holes establish an equilibrium Fermi energy $E_F(T)$. It is not obvious whether at $E_F(T)$ there will be a viable concentration of that charge state that leads to a nonvanishing magnetic moment. Previous authors have usually arbitrarily assumed a given charge state of the defects and proceeded to calculate its magnetic properties without examining if this is the stable charge state at E_F. Here, we take into account compensations and possible nonmagnetic charge states by first calculating for the magnetic defect (here, V_{Hf}) and for possible compensating defects (here, V_O) the defect formation enthalpies $\{\Delta H_{D,q}(E_F,\mu_\alpha)\}$ of the respective defect D in charge state q, as a function of the Fermi energy E_F and chemical potentials μ_α representing the growth condition (e.g., O-rich–Hf-poor). Next, we calculate, via compensation conditions the equilibrium Fermi energy $E_F(T_{\text{growth}},\mu)$ at a given growth temperature T_{growth} and the corresponding equilibrium concentrations $c(T_{\text{growth}},\mu_\alpha)$ of all defects. Finally, we calculate for these obtained concentrations the Fermi level at room temperature and the distribution of the magnetic and nonmagnetic charge states of the magnetic candidate defect. Only if this procedure predicts significant concentrations of the defect having nonzero magnetic moment can one proceed to expect defect-induced magnetism.

Third, having found how many stable moment-carrying defects exist, one must establish the range of magnetic defect-defect interaction d for the moment-carrying stable charge state. Indeed, a highly localized (deep-gap) defect orbital could lead to only a very-short-range defect-defect interaction that would fail to percolate through the sample, leading to a vanishing Curie temperature. To establish the range of magnetic interaction one needs to perform a magnetic calculation establishing an underlying interaction mechanism. Das Permmaraju and Sanvito[3] have examined the magnetic interaction of two $V^0_{\text{cation-IV}}$ in HfO_2 up to three-neighbor distance. Bouzerar and Ziman[7] have used the Hubbard-model Hamiltonian with an additional term to account for the perturbative potential due to randomly distributed cation vacancies inducing magnetic moments on neighboring oxygen sites. The existence of ferromagnetism depends strongly on the choice of the model parameters. In CaO, Elfimov *et al.*[1] have predicted the existence of nonzero local magnetic moments for $V^0_{\text{cation-II}}$, but have not calculated the range of magnetic interactions between two such vacancies; Osorio-Guillén *et al.*[6] have calculated that these vacancies interact ferromagnetically if they are separated by up to four-neighbor distance. Andriotis *et al.*[9–11] have found that for a C_{60} dimer the spin triplet is the ground state when two C vacancies are introduced per C_{60} molecule, but the authors did not calculate the range of magnetic interactions.

Fourth, given the defect-defect interaction range d determined above, one must establish the minimal percolation concentration $x_{\text{perc}}(\lambda,d)$ of defects (D,q) for the relevant lattice type λ (e.g., Baddelayite-type for HfO_2, NaCl-type for CaO). In general, the shorter the interaction range d, the larger the defect concentration required to establish wall-to-wall percolation and hence collective magnetism. However, calculations of the "percolation staircase" $x_{\text{perc}}(\lambda)$ vs d for general lattice structures λ are scarce, except for simple monoatomic cases.[20] Previous calculations[1,3] of defect-induced magnetism have generally not considered whether the percolation condition is satisfied or not. The main question is then: is the equilibrium concentration $c_{D,q}(T,\mu)$ of a magnetic-moment-carrying defect D at charge state q comparable to the percolation concentration $x_{\text{perc}}(\lambda,d)$ of the appropriated lattice type λ given its magnetic interaction range d?

In this paper we find that (i) the charge states of Hf vacancies which lead to nonzero magnetic moments are $q=0,1-,2-,3-$. (ii) The maximal equilibrium concentration of all charge states of Hf vacancies at growth temperature of $T_{\text{growth}}=2500$ K and $p(O_2)=100$ atm (this partial pressure is chosen to be close to O-rich growth conditions) is 1.3×10^{17} cm^{-3} ($x=4.5\times10^{-6}$%), but the maximal concentration of charge states with nonzero magnetic moments at room temperature is only 6.4×10^{15} cm^{-3} ($x=2.2\times10^{-7}$%). (iii) The range of ferromagnetic vacancy-vacancy interactions in HfO_2 is $d\approx5$ nearest neighbors. (iv) The minimal concentration needed to establish percolation for $d=d_{5\text{NN}}$ on the HfO_2 lattice is $x_{\text{perc}}=13.5$%. Thus, the calculated equilibrium Hf vacancy concentration of charge states which lead to nonzero magnetic moments falls short by eight orders of magnitude from the minimal percolation density. Thus, to

establish ferromagnetism in HfO_2 requires an enhancing factor of the uncompensated V_{Hf} concentration relative to equilibrium growth of the order of 10^8.

II. METHODS

A. Calculation of the magnetic configuration of a single vacancy

All total energies, atomic forces, and magnetic moments were calculated via first principles using the projector augmented wave method and the generalized gradient approximation (GGA-PBE) as implemented in the VASP code.[21] The energy cutoff in the planes wave expansion was 520 eV. All calculations for the neutral and charge vacancies were performed using a fully relaxed GGA host supercell which contains 96 atoms. Brillouin-zone integration was performed on a $2\times2\times2$ **k**-mesh with a Gaussian broadening for the atomic relaxation and a Γ-centered $4\times4\times4$ **k**-mesh using the tetrahedron method for the calculation of the total energies, charge density, magnetic moments, and square of the wave function in the chosen energy ranges.

B. Calculation of the formation enthalpies of vacancies and the equilibrium concentration of point defects

We calculate the formation enthalpy[22] $\Delta H_{D,q}(E_F,\mu)$ of defect D in charge state q (here, D=Hf or O vacancies) as a function of the Fermi energy E_F and the chemical potential μ of Hf and O:

$$\Delta H_{D,q}(E_F,\mu) = [E_{D,q} - E_H] + n_\alpha(\mu_\alpha^{\text{elem}} + \Delta\mu_\alpha) + q(E_v + \Delta E_F), \tag{1}$$

here, $E_{D,q}$ is the total energy of the supercell containing the defect D in charge state q and E_H is the energy of the pure host supercell. The second term in Eq. (1) describes the chemical reservoir of equilibrium, where $n_\alpha=\pm1$ if an atom is removed (+1) or added (−1); the chemical potential $\mu_\alpha=\mu_\alpha^{\text{elem}}+\Delta\mu_\alpha$ of the removed ion α (=Hf,O) is given with respect to the elemental phase. For the elemental reference μ_α^{elem}, we choose the solid phase except for oxygen, where we use the O_2 molecule. The third term in Eq. (1) is the energy of the electron reservoir—i.e., the Fermi energy $E_F=E_v+\Delta E_F$, which can range from the valence band maximum (VBM) (E_v)to the conduction band minimum (CBM) (E_c) and is determined by the equilibrium concentration of electrons and holes in the sample. Maintaining a system in thermodynamic equilibrium with bulk HfO_2 requires that $\Delta\mu_{Hf}+2\Delta\mu_O=\Delta H_f(HfO_2)$, where $\Delta H_f(HfO_2)=-10.75$ eV/f.u. is the calculated formation enthalpy of HfO_2. This condition leaves one free degree of freedom (μ_{Hf} or μ_O) for the chemical potentials of the constituents. Thus, growth conditions can be chosen between the limit of Hf-rich–O-poor $[\Delta\mu_{Hf}=0,\Delta\mu_O=\Delta H_f(HfO_2)/2]$ and the limit Hf-poor–O-rich $[\Delta\mu_{Hf}=\Delta H_f(HfO_2),\Delta\mu_O=0]$ conditions. In order to simulate realistic growth conditions, we include the enthalpy and entropy contributions to the oxygen chemical potential $\mu_O$in the O_2 gas phase at temperature T and pressure P. Using the tabulated[23] values (enthalpy H_0=8.7 kJ mol^{-1} and entropy S_0=205 J mol^{-1} K^{-1}) for O_2 at standard conditions, we express $\Delta\mu_O$ of Eq. (1) as

$$\Delta\mu_O(T,P) = \frac{1}{2}\{[H_0 + \Delta H(T)] - T[S_0 + \Delta S(T)]\} + \frac{1}{2}k_B T \ln\frac{P}{P_0}, \tag{2}$$

where $\Delta H(T)=C_P(T-T_0)$ and $\Delta S(T)=C_P\ln(T/T_0)$. Employing the ideal gas law for $T\geq298$ K, we use $C_P=3.5k_B$ for the constant-pressure heat capacity per diatomic molecule.

We correct the calculated formation enthalpies from finite supercell and GGA errors according to the following scheme.[22]. (i) *Supercell error corrections*: (a) *Band filling correction* is applied for shallow donors and acceptors; the use of finite-size supercells implies very high, degenerate doping densities far beyond the insulator-metal transition. The ensuing Moss-Burstein-like band filling effects raise artificially ΔH which needs to be corrected. (b) *Potential alignment correction*; this applies to charged impurities where violation of the charge-neutrality condition leads to divergence of the Coulomb potential. Here, the total energy calculated from the expression originally derived for charged-neutral systems[24] suffers from the same arbitrariness as single-particle energies.[22] This is corrected by an appropriate potential alignment procedure. (c) *Image charge correction*, performed for charged defects. Here, the effective (i.e., screened) Madelung energy of the defect charge in the jellium background is corrected to $O(L^5)$, according to Ref. 25. (ii) *GGA error corrections*: (a) *GGA band gap correction*; the GGA band gap of HfO_2 is 3.93 eV, a much smaller value than the experimental gap (5.45 eV). We correct this discrepancy with the (temperature-dependent) experimental gap by shifting the CBM energy. (b) *Shallow donor and acceptor correction*, since the wave functions of shallow donors or acceptors are perturbed host states rather than defect localized states, the respective energies of the donor and acceptor states are expected to follow the corrections of the CBM and VBM. For HfO_2 the Hf vacancy is shallow but we have not shifted the VBM, so $\Delta E_v=0$. On the other hand, as the oxygen vacancy is deep in nature, this correction is not applied to this defect.

The equilibrium defect concentration is calculated from the defect formation enthalpies and using the Boltzmann distribution

$$c_{D,q}(E_F,\mu,T) = N\exp[-\Delta H_{D,q}(E_F,\mu)/\kappa T], \tag{3}$$

where N is the concentration of atomic sites that are substituted by the vacancy. The chemical potential μ corresponds to the growth conditions described above, and T is the growth temperature. Since the vacancy concentration depends explicitly on E_F and since E_F depends on the concentration of charged vacancies and free carriers (by means of the requirement of overall charge neutrality), then these variables ($c_{D,q}$, E_F, carrier concentration) are calculated self-consistently. Here, the electron and hole concentrations are calculated as a function of E_F and T by numerical integration of the Fermi-Dirac distribution using an effective-mass-like approximation for the host bands.

C. Calculation of the magnetic interaction range

To quantify the ferromagnetic interaction we calculated the ferromagnetic stabilization energy $\Delta E_{\mathrm{FM}}(d)=E_{\mathrm{AFM}}(d)-E_{\mathrm{FM}}(d)$ by placing two V_{Hf}^{0} defects at separation d in the supercell and calculate via GGA the difference between the ferromagnetic (FM) and antiferromagnetic (AFM) total energies where all atomic positions are relaxed.

D. Calculation of the percolation staircase

The calculation of the percolation staircase is done (as described in the Appendix) considering vacancies that randomly occupy the sites of an infinite periodic lattice λ with occupation probability (concentration) $x=c[V]/N$, where N is the total number of sites. Two such vacancies interact if they are separated by less than distance d. We find the percolation threshold function $x_{\mathrm{perc}}(\lambda,d)$ by a finite-size analysis of Monte Carlo simulation results. Since $x_{\mathrm{perc}}(\lambda,d)$ may change its value only at the discrete values of $d=d_{1\mathrm{NN}},d_{2\mathrm{NN}},\ldots,d_{n\mathrm{NN}},\ldots$ (where $d_{n\mathrm{NN}}$ is the nth nearest-neighbor separation on the lattice λ), we enumerate $d_{n\mathrm{NN}}$ up to a given maximum separation. Then, for each $d_{n\mathrm{NN}}$ and a given value of linear dimension L of a finite-size lattice λ (the final results are not sensitive to the precise definition of L), we build an appropriate neighbor table and use it to identify whether an arbitrary configuration of vacancies contains a spanning cluster (that is, a cluster that crosses the system from one side to an opposite side).

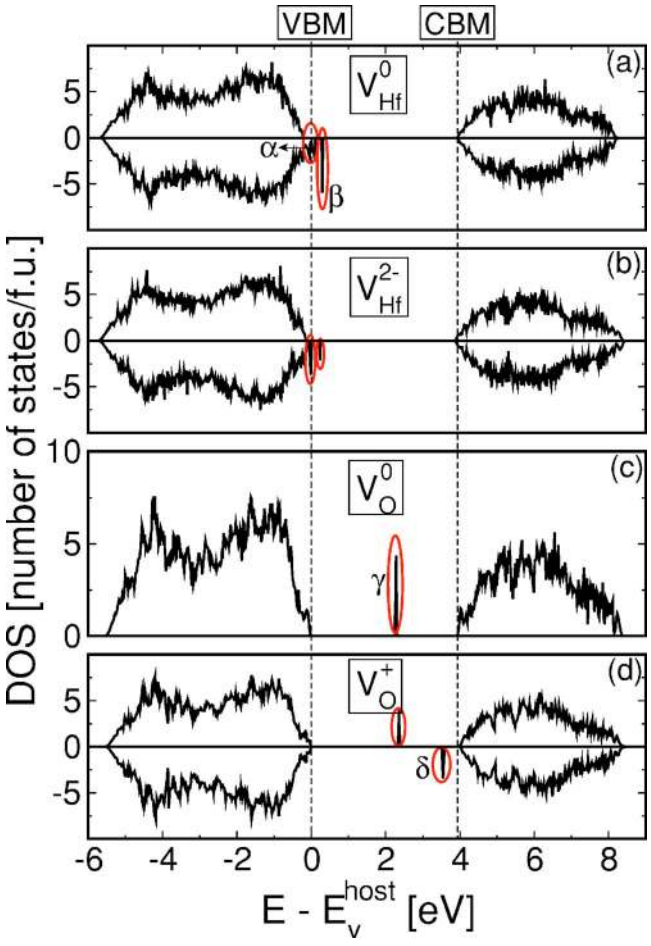

FIG. 1. (Color online) Calculated total density of states (DOS), for two charge states of the Hf vacancy; V_{Hf}^{0} and V_{Hf}^{2-}, and two charge states of the O vacancy, V_{O}^{0} and V_{O}^{+}. Spin up and spin down are depicted as upper and lower panels, respectively. The vertical dashed lines represent the VBM and CBM of the host crystal. The red ellipses highlight features for which we give the square of the wave function in Fig. 2.

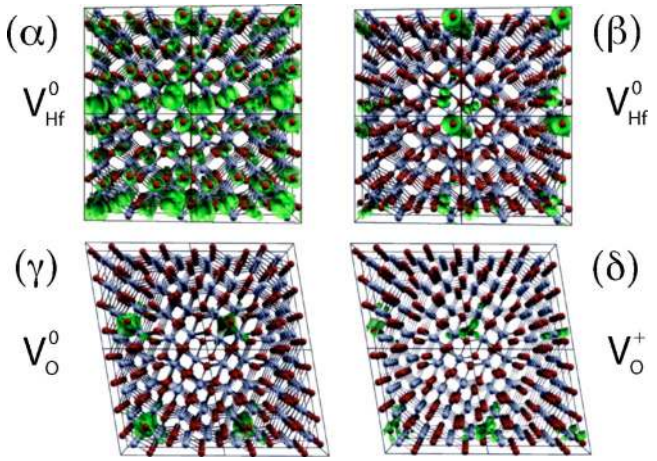

FIG. 2. (Color online) The square wave functions for the states α, β, γ, and δ enclosed by red ellipses and labeled in Fig. 1. Gray and red circles represent Hf and O atoms, respectively. The green isosurface represents the wave function.

III. RESULTS

A. Results for the magnetic configuration of single Hf and O vacancies in different charge states

Figures 1(a) and 1(b) show the total density of states (DOS) for the Hf vacancy in charge states V_{Hf}^{0} and V_{Hf}^{2-}. We see that the removal of a single Hf atom introduces unoccupied but spin-polarized states above the VBM for V_{Hf}^{0} and V_{Hf}^{2-} (enclosed by the red ellipses). The integrated DOS (not shown) gives four empty states for V_{Hf}^{0} and two empty states for V_{Hf}^{2-}. The four empty states introduced by V_{Hf}^{0} account for the calculated local magnetic moment of $4\mu_B$. Figure 2 (α) and (β) shows the square of the wave function for these four spin-polarized states in the energy range from $E_V-0.2$ eV to $E_V+0.07$ eV and $E_V+0.14$ eV to $E_V+0.22$ eV, respectively. It can be seen that the three empty states labeled α in Fig. 1(a) which are close to the VBM are delocalized, whereas the empty state labeled β in Fig. 1(b) inside the gap is more localized. Successive filling of these four empty levels leads to a decrease of the local magnetic moment up to the unpolarized situation for V_{Hf}^{4-}.

Figures 1(c) and 1(d) show the total DOS for oxygen vacancy charge states V_{O}^{0} and V_{O}^{+}. In the neutral state this defect introduces a fully occupied spin-unpolarized mid gap state, and in the single positive charged state it introduces a spin-polarized mid gap state, resulting in a local magnetic moment of $1\mu_B$. Figure 2 (γ) and (δ) shows the square of the wave function of the states γ for V_{O}^{0} and δ for V_{O}^{+} in Figs.

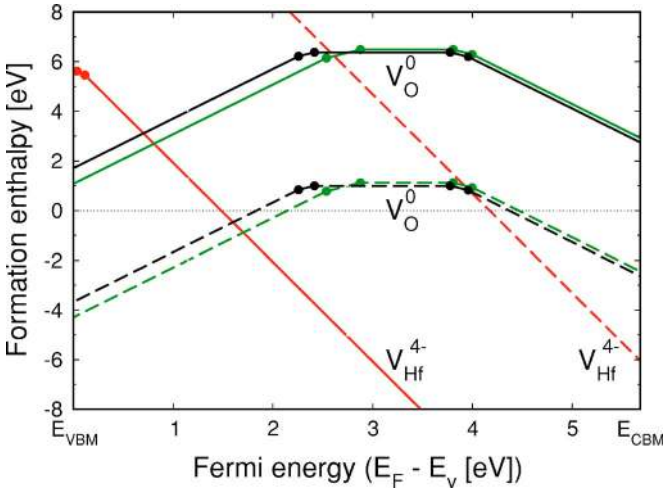

FIG. 3. (Color online) Calculated formation enthalpies for isolated anion and cation vacancies in HfO_2 in different charge states. Dashed lines denote Hf-rich–O-poor condition ($\Delta\mu_{Hf}=0$) whereas solid lines denote Hf-poor–O-rich condition ($\Delta\mu_{Hf}=-10.75$ eV) chemical potentials. Since there are two different crystallographic sites for O in the HfO_2 lattice, we show two lines: green lines represent O type 1 and black lines O type 2. Solid dots represent the transition energies between different charge states.

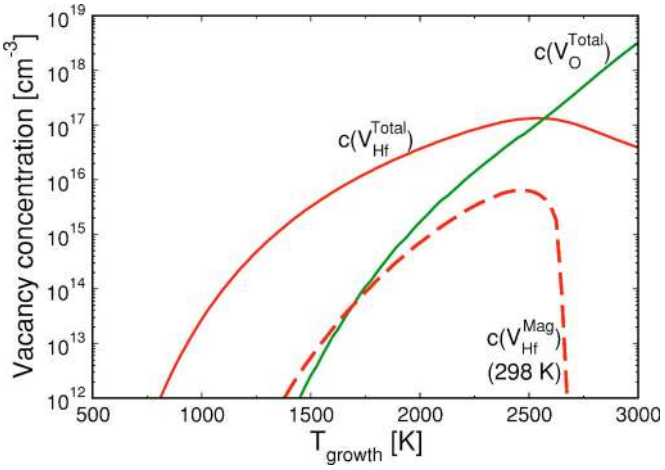

FIG. 4. (Color online) Calculated total vacancy concentrations for Hf, $c(V_{Hf}^{Total})$, and oxygen, $c(V_O^{Total})$, vacancy at growth conditions defined by Eq. (2) with $p(O_2)=100$ atm. $c(V_{Hf}^{Total})$ is the calculated concentration of moment-carrying states.

1(c) and 1(d), respectively. These gap states are very localized and well below the CBM, showing that the polaron model (requiring an overlap of this level with the conduction band) is not fulfilled.

B. Results for the formation enthalpies and transition energies of Hf and O vacancies and equilibrium concentration of magnetic defects in HfO_2

Figure 3 shows the formation enthalpies as a function of Fermi energy for Hf and O vacancies in HfO_2. Under Hf-rich growth conditions (dashed lines) and for all values of the Fermi energy, the nonmagnetic defects of $V_O^q(q=-2,0,2+)$ and V_{Hf}^{4-} have a lower formation energy and hence higher concentration than the magnetic defects $V_{Hf}^q(q=0,1-,2-,3-)$. This is also true for Hf-poor conditions (solid lines), where the nonmagnetic defects of V_O^{2+} and V_{Hf}^{4-} have lower formation energy for all Fermi levels. As the formation enthalpy of the magnetic defects V_{Hf}^q $(q=0,1-,2-,3-)$ is rather high even for the Hf-poor growth conditions, this implies a very small concentration of those under equilibrium conditions—i.e., when the defect densities are in equilibrium with the chemical reservoir at sufficiently high growth temperatures: e.g., $T>1000$ K. At room temperature, the equilibrium of the defect density is generally not established, but the density of the electronic system generally is; i.e., a new Fermi level will be established when the defect densities for the high growth temperature are "frozen-in" during the cooldown to room temperature. As a result, a new distribution between magnetic and nonmagnetic charge states will be reached (see below). Our calculated formation enthalpy for V_{Hf}^0 under Hf-poor conditions is 5.62 eV, in good agreement with the value calculated by Foster *et al.*[26] of 5.7 eV using Vanderbilt ultrasoft pseudopotentials and GGA-PW92.

For the cases of anion vacancies, we can see from Fig. 3 that V_O is amphoteric, having both donor and acceptor levels in the gap. The formation enthalpies for V_O^0 at the two types of oxygen sites are 6.49 eV and 6.37 eV, respectively, at Hf-poor conditions. These values are in good agreement with the calculation by Scopel *et al.*,[27] yielding 6.38 eV. Foster *et al.*[26] calculated 9.36 eV and 9.34 eV for V_O^0 for the two types of oxygen sites. Note that if we would treat V_O as a shallow donor (the calculation of the formation enthalpy of V_O^0 is corrected by the shift of the conduction band), our calculated formation enthalpies become 9.99 eV and 9.87 eV due to the shallow donor-acceptor correction,[22] which agrees with the values in Ref. 26. However, this is not a correct assumption since the calculated DOS (Fig. 1) shows that V_O^0 introduces fully occupied midgap states, which suggest that V_O should be considered as a deep donor. This treatment agrees with the findings in hybrid functional calculations by Gavartin *et al.*.[28] Also, we can observe from Fig. 3 that all five charge states of the O vacancy exist as stable states for some Fermi energies,[28] contrasting the negative-U character found by other authors[29,30] for O vacancies in cubic[29] HfO_2 and tetragonal[30] HfO_2.

Figure 4 shows the calculated anion and cation total vacancy concentrations of HfO_2, $c(V_O^{Total})$, and $c(V_{Hf}^{Total})$ and the concentration of moment-carrying states $c(V_{Hf}^{Mag})$ at room temperature as well. $c(V_{Hf}^{Total})$ and $c(V_O^{Total})$ are calculated taking into account the dependence of the chemical potential $\Delta\mu_O$ on T and P in the gas phase of O_2 [Eq. (2)]. The total maximal concentration of Hf vacancies at $T=2500$ K and $p(O_2)=100$ atm is 1.3×10^{17} cm^{-3} ($x=4.5\times10^{-6}$%). Due to the reduction of $\Delta\mu_O$ with increasing temperature [see Eq. (2)], $c(V_{Hf}^{Total})$ starts to decrease and $c(V_O^{Total})$ strongly increases beyond $T=2500$ K. At temperatures higher than $T=2800$ K the concentration of oxygen vacancies becomes higher that Hf vacancies. $c(V_{Hf}^{Mag})$ at room temperature reaches a maximum of 6.4×10^{15} cm^{-3} ($x=2.2\times10^{-7}$%) at $T_{growth}=2450$ K, being at least two orders of magnitude

TABLE I. Calculated ferromagnetic stabilization energy ($\Delta E_{\mathrm{FM}}=E_{\mathrm{AFM}}-E_{\mathrm{FM}}$) as a function of Hf vacancy pair distance (d_{ij}).

R_n	d_{ij} (Å)	ΔE_{FM} (meV)
$R_{1a\mathrm{NN}}$	3.425	205
$R_{1b\mathrm{NN}}$	3.437	66
$R_{3\mathrm{NN}}$	4.538	51
$R_{5\mathrm{NN}}$	5.937	39

lower than $c(V_{\mathrm{Hf}}^{\mathrm{Total}})$. This is due to either the ionization of holes into the non-spin-polarized valence band ($T_{\mathrm{growth}}<2000$ K) or due to compensation by V_{O}^{2+} ($T_{\mathrm{growth}}>2000$ K).

C. Results for the range of V_{Hf}-V_{Hf} magnetic interactions in HfO_2

Table I gives the ferromagnetic stabilization energy $\Delta E_{\mathrm{FM}}(d)=E_{\mathrm{AFM}}(d)-E_{\mathrm{FM}}(d)$ obtained by placing two V_{Hf}^{0} defects at separation d in a 96-atom supercell. We see that the stabilization energy is rather strong for the first neighbors and then it starts to decrease rapidly. At the first neighbor the ferromagnetic stabilization energy is 205 meV and at the "fifth" neighbor (see below, Sec. III D) the ferromagnetic stabilization energy is 39 meV. We further considered the moment-carrying V_{O}^{-} state ($\mu=1\mu_B$) of the oxygen vacancy as a possible source of ferromagnetism. We find, however, antiferromagnetic coupling—e.g., $\Delta E_{\mathrm{FM}}(d)=-74$ meV for close vacancy pairs with $d=2.6$ Å (sharing two cations), falling off to $\Delta E_{\mathrm{FM}}(d)=-8$ meV for more distant pairs with $d=6.4$ Å. Thus, we conclude that oxygen vacancies are not responsible for ferromagnetism.

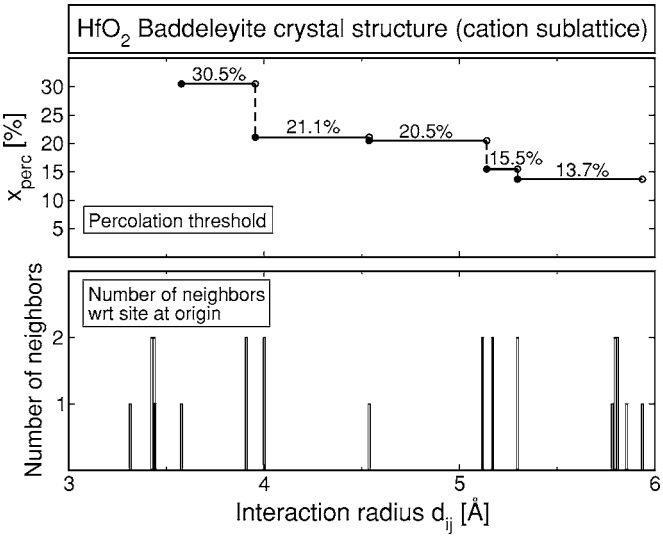

FIG. 5. Percolation threshold and number of nearest neighbors (NN) vs cation-cation distance. Due to the complexity of the Baddelayite structure, some shells are averaged out to a single one for the calculation of the percolation thresholds (see Sec. III D).

D. Results for the percolation threshold for the cation sublattice of the HfO_2 Baddelayite structure

Figure 5 shows the calculated percolation threshold staircase and the cationic shell structure of HfO_2. The cationic shell structure is rather complex in the Baddelayite structure in comparison with other oxides (e.g., CaO, TiO_2). The Baddelayite structure shows 16 shells at a distance less than 6 Å, where some of then can be considered as "degenerate"; i.e., the distance between different shells is less than 0.25 Å. For all the shells the numbers of neighbors is not larger than two atoms. Due to the complexity of this structure, we have averaged out some of the shells that fall in our "degenerate" definition to carry out the calculation of the percolation thresholds. From the percolation staircase we can see that the minimal Hf vacancy concentration needed to establish percolation on the HfO_2 lattice at $d=d_{1\mathrm{NN}}$ is $x=30.5\%$. This minimal concentration falls when the distance of the interaction between two Hf vacancies increases. We have calculated the minimal concentration needed to establish percolation up to the fifth shell, where this concentration is $x=13.5\%$ on the HfO_2 lattice. Thus, the calculated equilibrium Hf vacancy concentration of charge states which lead to nonzero magnetic moments falls short by eight orders of magnitude from the minimal percolation density. Thus, to establish ferromagnetism in HfO_2 requires an enhancing factor of defect concentrations relative to equilibrium of the order of 10^8.

IV. CONCLUSION

The theoretical prediction of ferromagnetic semiconductors or insulators requires the assessment of several conditions, concerning the deviation from the ideal host lattice, which need to be met simultaneously. We addressed these conditions in a case study of ferromagnetism in HfO_2 without magnetic ions: (i) Which defects in which charge states carry a magnetic moment and, thus, are candidates to promote ferromagnetism? (ii) What is the concentration of these magnetic-moment-carrying states when considering real materials conditions—e.g., equilibrium growth under realistic conditions and the formation of compensating defects which may eliminate the magnetic charge states? (iii) What is the range of interactions of the magnetic defects? (iv) What is the concentration needed for magnetic percolation given the range of interactions? Under realistic growth conditions, can this concentration be achieved for the magnetic defects in their moment-carrying charge state? In HfO_2, we find that both types of lattice vacancies do have specific charge states in which they carry magnetic moments. A ferromagnetic pair interaction exists, however, only in the case of V_{Hf}. The equilibrium concentration of V_{Hf} in moment-carrying states is much lower than the concentration needed for magnetic percolation.

ACKNOWLEDGMENT

This work was funded by DARPA under NREL Contract No. DE-AC36-99GO10337

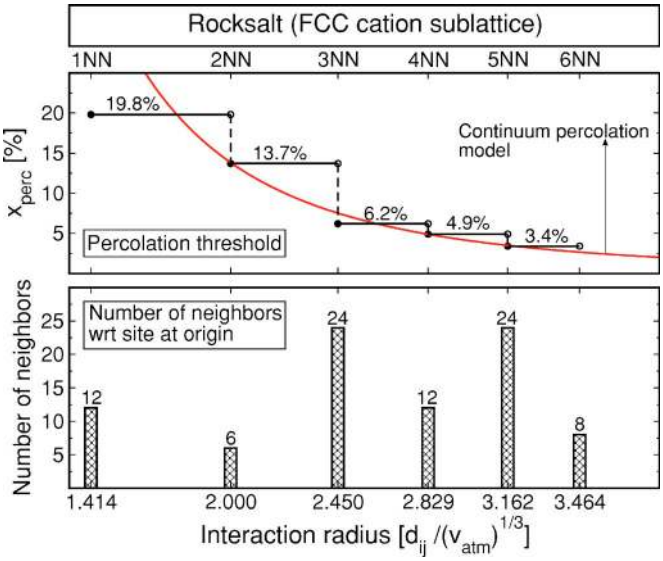

FIG. 6. (Color online) Percolation threshold and number of nearest neighbors (NN) vs cation-cation distance for the rocksalt crystal structure (fcc) cation sublattice.

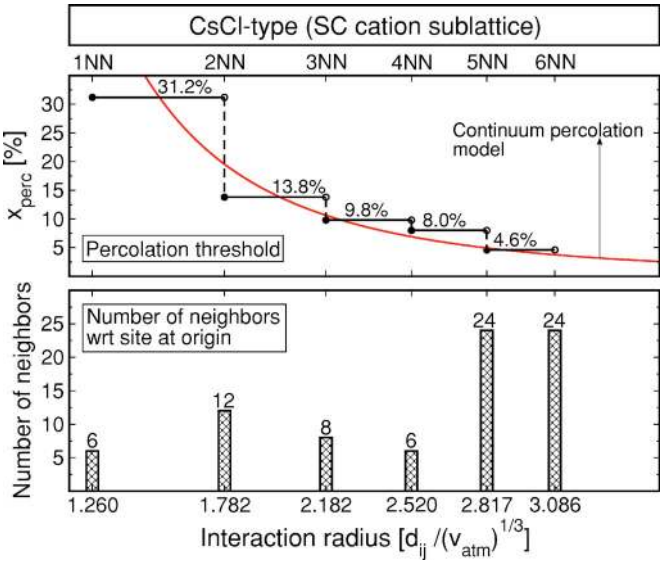

FIG. 8. (Color online) Percolation threshold and number of nearest neighbors (NN) vs cation-cation distance for the CsCl crystal structure (sc) cation sublattice.

APPENDIX: PERCOLATION STAIRCASES IN COMMON LATTICES

Substitution of the host lattice sites by guest atoms X generally leads to modification of the system properties. Notable examples include impurity doping of semiconductors leading to electrical conductivity,[31,32] substitution of the nonmagnetic host by magnetic ions leading to ferromagnetism,[33] the formation of bond length anomalies upon isovalent alloying,[34] and the appearance of new phonon bands upon alloying light-mass impurities in heavy-mass host lattices.[35] A special type of property change upon alloying or doping occurs when the interaction between the guest atom X leads to the onset of a macroscopic effect when the interacting atoms form an infinite connected cluster.[20] When this happens we say that the interaction percolates the system. Whereas any amount of substitution of the host by X can lead to some property change, the occurrence of "wall-to-wall" percolation leads to the onset of *collective* effects, such as the formation of metallic impurity bands,[31,32] collective ferromagnetism,[33] bond length singularities,[34] and phonon anomalies and anomalous microhardness.[36–40]

The smallest concentration x_{perc} sufficient for establishing percolation is called the percolation threshold. Clearly, the value of $x_{\mathrm{perc}}^{\lambda,n}$ depends on lattice type λ (fcc, bcc, sc, etc.) through its topological site connectivity and on the interaction radius R_n within which an X atom "sees" another atom

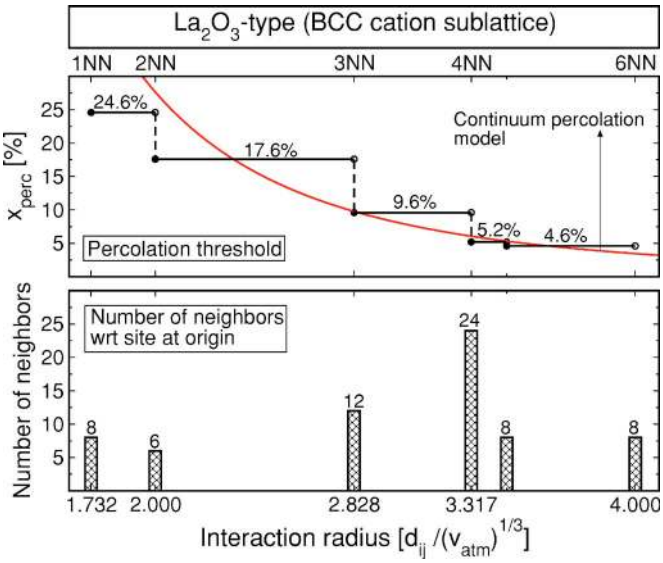

FIG. 7. (Color online) Percolation threshold and number of nearest neighbors (NN) vs cation-cation distance for the La_2O_3 crystal structure (bcc) cation sublattice.

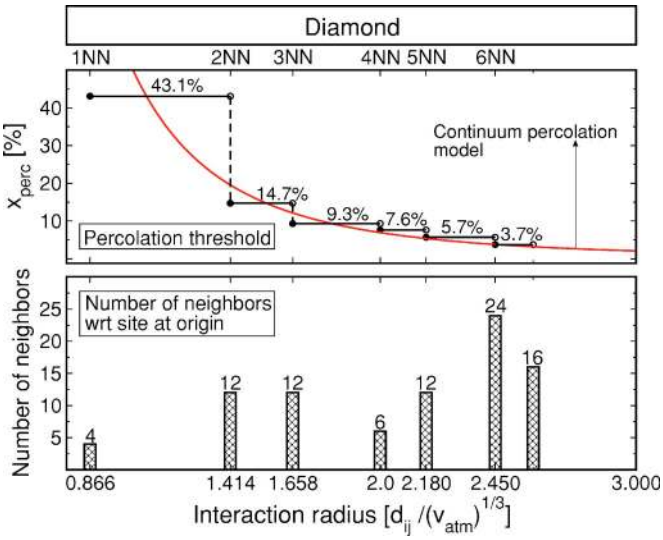

FIG. 9. (Color online) Percolation threshold and number of nearest neighbors (NN) vs cation-cation distance for the diamond crystal structure.

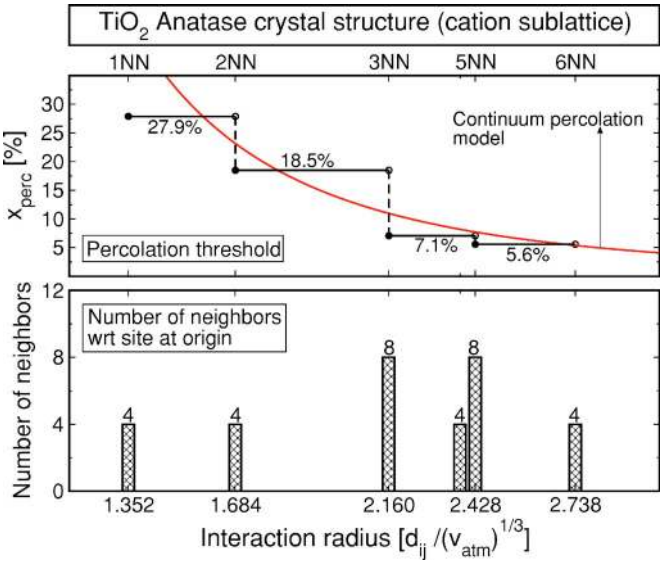

FIG. 10. (Color online) Percolation threshold and number of nearest neighbors (NN) vs cation-cation distance for the anatase crystal structure cation sublattice.

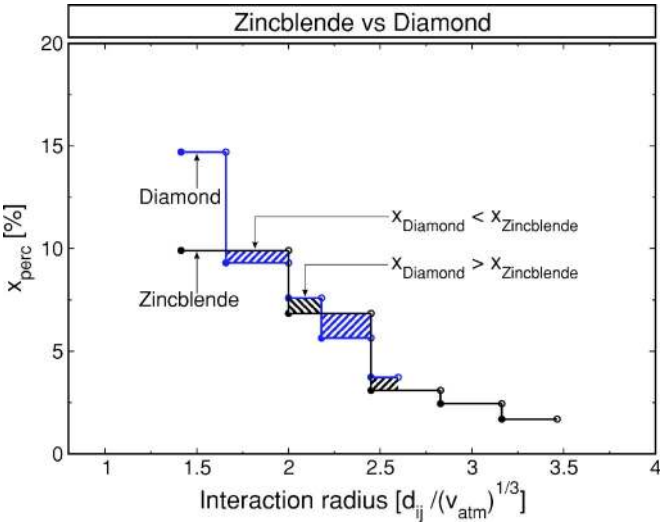

FIG. 11. (Color online) Comparison between the percolation thresholds of zinc blende versus diamond.

X. The interaction radius depends in turn on the physical property being considered. While for mechanical properties[34] R_n might be confined to the atomic radius of X (and thus percolation exists when nearest neighbors form a continuous cluster), for magnetic X-X interactions R_n might be the range of the Heisenberg exchange between the magnetic ions, and it can extend to 5–15 neighbors.[6,41,42]

In the past $x_{\text{perc}}^{\lambda,n}$ was calculated for many types of discrete problems (site and bond percolation, directed percolation, bootstrap percolation, etc.) for simple lattices such as λ =fcc, bcc, sc and mostly for n=first nearest neighbors.[43,44] Two types of methods for estimating x_{perc} have been used: analytic (series expansion, ϵ expansion, etc.) and Monte Carlo. We will use the Monte Carlo method since it can be applied it to arbitrary lattices with arbitrary interaction distance. We restrict this study to an analysis of percolation and will not analyze other critical properties.

Method of calculation. Consider guest atoms X that randomly occupy the sites of an infinite periodic lattice λ with occupation probability (concentration) x. Two atoms X interact if they are separated by less than[45] R_n. Our model is a generalization of the classical site percolation model[20] (in which R_n is just the nearest-neighbor distance) and could serve to describe, for example, ferromagnetism in dilute magnetic semiconductors,[33] in which the range R_n of exchange interactions between the magnetic ions is much larger than the nearest-neighbor distance.[6,41,42] On a given lattice λ, we find the percolation threshold function $x_{\text{perc}}^{\lambda,n}$ by a finite-size analysis of Monte Carlo simulation results. Since $x_{\text{perc}}^{\lambda,n}$ may change its value only at the discrete values of $R_n = R_{1\text{NN}}, R_{2\text{NN}}, \ldots, R_{n\text{NN}}, \ldots$ (where $R_{n\text{NN}}$ is the nth nearest-neighbor separation on the lattice λ), we begin by enumerating $R_{n\text{NN}}$ up to a given maximum separation. For each $R_{n\text{NN}}$ and a given value of linear dimension L of a finite-size lattice λ (the final results are not sensitive to the precise definition of L), we build an appropriate neighbor table and use it to identify[46] whether an arbitrary configuration of X atoms contains a spanning cluster (that is, a cluster that crosses the system from one side to an opposite side). Then, for a trial occupation probability x, we find the spanning probability $\Pi(x,L)$. One way to implement a finite-size scaling analysis is to define an "effective" percolation threshold $x_{\text{eff}}(L,\Pi_0)$ by $\Pi(x,L)=\Pi_0$ for an arbitrary fixed value of $\Pi_0 \approx 1/2$. Then, one can identify x_{perc} by plotting x_{eff} vs $L^{-1/\nu}$ (where ν is the so-called correlation-length critical exponent[20]) and using the scaling relation[20]

$$x_{\text{eff}}(L,\Pi_0) - x_{\text{perc}} \propto L^{-1/\nu}. \tag{A1}$$

Here, we use a different version of this analysis by noting that if one selects as the value of Π_0 the infinite system spanning probability Π_∞, then (assuming $0<\Pi_\infty<1$), up to the same higher-order terms as in Eq. (A1), the true and the "effective" percolation thresholds are equal: $x_{\text{eff}}(L,\Pi_\infty) \cong x_{\text{perc}}$=const, and

$$\Pi(x = x_{\text{perc}}, L) = \Pi_\infty = \text{const}. \tag{A2}$$

Thus, we begin with some trial occupation probability x and search for the value of x at which $\Pi(x,L)$ becomes size independent.[47,48] This allows us to gradually increase the statistical precision (number of Monte Carlo trials), using the highest precision only as necessary for the values of x very close to x_{perc}.

The above discussion pertains to percolation on one sublattice. For example, the cation sublattice of zinc-blende GaAs and the cation sublattice of rocksalt CaO both exhibit fcc percolation. The results for $x_{\text{perc}}^{\lambda,n}$ vs R_n of such single sublattices are shown in Figs. 6–10. We can consider also a case of percolation on more than a single sublattice. For example, at temperatures where the A-type and B-type lattices of $A_{1-x}B_x$ fcc alloy become completely random, an impurity X can substitute interchangeably on either site. For such cases in which a parent multisite lattice $\tilde{\lambda}$ can be subdivided into $N \geq 1$ periodic sublattices $\lambda_1, \ldots, \lambda_N$ and impu-

rities occupy only a subset $\lambda=\lambda_i\cup\cdots\cup\lambda_j$ of those sublattices (where $\{i,\ldots,j\}\subset\{1,\ldots,N\}$). This corresponds to an impurity atom X substituting for only a particular constituent in an ordered compound, whereas different choices of λ for a fixed $\tilde{\lambda}$ correspond to either different types of ordering or to order-disorder transitions. The numerical procedure for finding the percolation threshold remains unchanged; however, we will define $\tilde{x}_{\mathrm{perc}}$ as the average concentration of impurities with respect to the parent lattice $\tilde{\lambda}$, so as to be able to compare the results for different types of ordering of the same amount of impurity atoms. The results for such pairs are shown in Fig. 11.

[1] I. S. Elfimov, S. Yunoki, and G. A. Sawatzky, Phys. Rev. Lett. **89**, 216403 (2002).
[2] M. Venkatesan, C. Fitzgerald, and J. Coey, Nature (London) **430**, 630 (2004).
[3] C. Das Pemmaraju and S. Sanvito, Phys. Rev. Lett. **94**, 217205 (2005).
[4] J. Coey, M. Venkatesan, and C. Fitzgerald, Nat. Mater. **4**, 173 (2005).
[5] J. M. D. Coey, M. Venkatesan, P. Stamenov, C. B. Fitzgerald, and L. S. Dorneles, Phys. Rev. B **72**, 024450 (2005).
[6] J. Osorio-Guillén, S. Lany, S. V. Barabash, and A. Zunger, Phys. Rev. Lett. **96**, 107203 (2006).
[7] G. Bouzerar and T. Ziman, Phys. Rev. Lett. **96**, 207602 (2006).
[8] H. Weng and J. Dong, Phys. Rev. B **73**, 132410 (2006).
[9] A. N. Andriotis, M. Menon, R. M. Sheetz, and L. Chernozatonskii, Phys. Rev. Lett. **90**, 026801 (2003).
[10] A. Andriotis, R. Sheetz, E. Richter, and M. Menon, Europhys. Lett. **72**, 658 (2005).
[11] A. Andriotis, M. Menon, R. Sheetz, and E. Richter, *Carbon-Based Magnetism* (Elsevier, Amsterdam, 2006), p. 483.
[12] N. H. Hong, J. Sakai, N. Poirot, and V. Brizé, Phys. Rev. B **73**, 132404 (2006).
[13] A. Sundaresan, R. Bhargavi, N. Rangarajan, U. Siddesh, and C. N. R. Rao, Phys. Rev. B **74**, 161306(R) (2006).
[14] G. Watkins, *Radiation Damage in Semiconductors* (Dunod, Paris, 1964).
[15] A. Stoneham, *Theory of Defects in Solids* (Clarendon, Oxford, 1975).
[16] M. Abraham, Y. Chen, L. Boatner, and R. Reynolds, Solid State Commun. **16**, 1209 (1975).
[17] B. Rose and L. Halliburton, J. Phys. C **7**, 3981 (1974).
[18] T. Kaspar *et al.*, Phys. Rev. B **73**, 155327 (2006).
[19] L.-H. Ye and A. J. Freeman, Phys. Rev. B **73**, 081304(R) (2006).
[20] D. Stauffer and A. Aharony, *Introduction to Percolation Theory*, 2nd ed. (Taylor and Francis, London, 1992).
[21] G. Kresse and D. Joubert, Phys. Rev. B **59**, 1758 (1999).
[22] C. Persson, Y.-J. Zhao, S. Lany, and A. Zunger, Phys. Rev. B **72**, 035211 (2005).
[23] R. Weast and M. Astle, *CRC Handbook of Chemistry and Physics*, 60th ed. (CRC Press, Boca Raton, FL, 1979).
[24] J. Ihm, A. Zunger, and M. Cohen, J. Phys. C **12**, 4409 (1979).
[25] G. Makov and M. C. Payne, Phys. Rev. B **51**, 4014 (1995).
[26] A. S. Foster, F. Lopez Gejo, A. L. Shluger, and R. M. Nieminen, Phys. Rev. B **65**, 174117 (2002).
[27] W. Scopel, A. da Silva, W. Orellana, and A. Fazzio, Appl. Phys. Lett. **84**, 1492 (2004).
[28] J. Gavartin, D. M. nos Ramo, A. Shluger, G. Bersuker, and B. Lee, Appl. Phys. Lett. **89**, 082908 (2006).
[29] Y. Feng, A. Kim, and M. Li, Appl. Phys. Lett. **87**, 062105 (2005).
[30] K. Xiong, J. Robertson, M. Gibson, and S. Clark, Appl. Phys. Lett. **87**, 183505 (2005).
[31] N. Mott, *Metal-insulator Transitions* (Taylor and Francis, London, 1974).
[32] E. Schubert, *Doping in III-V Semiconductors* (Cambridge University Press, Cambridge, England, 1993).
[33] T. Jungwirth, J. Sinova, J. Mašek, J. Kučera, and A. MacDonald, Rev. Mod. Phys. **78**, 809 (2006).
[34] L. Bellaiche, S.-H. Wei, and A. Zunger, Phys. Rev. B **56**, 13872 (1997).
[35] O. Pages, T. Tite, K. Kim, P. Graf, O. Maksimov, and M. Tamargo, J. Phys.: Condens. Matter **18**, 577 (2006).
[36] E. Rogacheva, Inorg. Chem. **33**, 1130 (1997).
[37] E. Rogacheva, A. Sologubenko, and I. Krivul'kin, Inorg. Chem. **34**, 545 (1998).
[38] E. Rogacheva, T. Tavrina, and I. Krivul'kin, Inorg. Chem. **35**, 236 (1999).
[39] E. Rogacheva, J. Phys. Chem. Solids **64**, 1579 (2003).
[40] E. Rogacheva, J. Phys. Chem. Solids **66**, 2104 (2005).
[41] A. Franceschetti, S. V. Dudiy, S. V. Barabash, A. Zunger, J. Xu, and M. van Schilfgaarde, Phys. Rev. Lett. **97**, 047202 (2006).
[42] L. Bergqvist, O. Eriksson, J. Kudrnovský, V. Drchal, P. Korzhavyi, and I. Turek, Phys. Rev. Lett. **93**, 137202 (2004).
[43] B. I. Halperin, S. Feng, and P. N. Sen, Phys. Rev. Lett. **54**, 2391 (1985).
[44] S. Feng, B. I. Halperin, and P. N. Sen, Phys. Rev. B **35**, 197 (1987).
[45] Note that this definition differs from the one in the model of "overlapping spheres" of radius R. In the latter, two spheres "interact" whenever their separation is less than $2R$.
[46] J. Hoshen and R. Kopelman, Phys. Rev. B **14**, 3438 (1976).
[47] Note that the $L\to\infty$ value of the spanning probability Π_∞ may differ depending on the details of the calculation setup such as the relative shape of the lattice unit cell and the Monte Carlo box; however, the resulting x_{perc} is insensitive to those details.
[48] J. Cardy, J. Phys. A **25**, L201 (1992).